A surface and a gas-phase mechanism for the description of growth on the diamond(100) surface in an oxy-acetylene torch reactor

A surface and a gas-phase mechanism for the description of growth on the diamond(100) surface in an oxy-acetylene torch reactor

M. Okkerse
Laboratorium voor Chemische Technologie, Eindhoven University of Technology, Postbus 513, 5600 MB Eindhoven and Kramers Laboratorium voor Fysische Technologie, Delft University of Technology, Prins Bernhardlaan 6, 2628 BW Delft, The Netherlands

M. H. J. M. de Croon[a)]
Laboratorium voor Chemische Technologie, Eindhoven University of Technology, Postbus 513, 5600 MB Eindhoven, The Netherlands

C. R. Kleijn and H. E. A. van den Akker
Kramers Laboratorium voor Fysische Technologie, Delft University of Technology, Prins Bernhardlaan 6, 2628 BW Delft, The Netherlands

G. B. Marin
Laboratorium voor Petrochemische Techniek, University of Ghent, Krijgslaan 281, B-9000 Gent, Belgium

(Received 29 September 1997; accepted for publication 1 September 1998)

A gas-phase and a surface mechanism were developed, suitable for multidimensional simulations of diamond oxy-acetylene torch reactors. The gas-phase mechanism was obtained by reducing a 48 species combustion chemistry mechanism to a 27 species mechanism with the aid of sensitivity analysis. The surface mechanism for growth on monocrystalline (100) surfaces developed, was based on literature quantum-mechanical calculations by Skokov *et al.* It consists of 67 elementary reaction steps and 41 species, and contains CH_3 and C_2H_2 as gas-phase growth precursors and atomic hydrogen and oxygen to etch carbon from the surface. The gas-phase and surface chemistry models were tested in one-dimensional simulations, yielding dependencies of the growth rate on feed composition and surface temperature that are in qualitative agreement with the experiments. A more detailed study of the surface chemistry showed that, compared to CH_3, acetylene contributes very little to diamond growth. Furthermore, molecular and atomic oxygen do not affect the diamond surface as much as atomic hydrogen because of their low concentrations. © *1998 American Institute of Physics.* [S0021-8979(98)05423-1]

I. INTRODUCTION

The unique properties of diamond[1] make it an attractive candidate for a variety of industrial applications. In particular single-crystalline diamond is a promising material for electronic applications.[2] The greatest barrier for exploitation is that centimeter size, single-crystalline diamond films are not readily available on the market. With oxy-acetylene combustion chemical vapor deposition (CVD) monocrystalline diamond layers can be grown at high growth rates and low cost.[3] However, the area of monocrystalline growth obtained by means of oxy-acetylene combustion CVD is as yet limited to about 20 mm^2. To be able to produce centimeter size monocrystalline diamond layers, the process has to be scaled up.

With the increasing capabilities of computational fluid dynamics and computational chemistry and with the increase of computing power, it has become possible to simulate the hydrodynamics and chemistry of CVD from first principles, leading to a more reliable design and a clearer understanding.[4] This requires a gas-phase and a surface chemistry model that, on the one hand, should be compact enough to keep computational demands at a reasonable level while, on the other, these models should be detailed enough to predict all the important aspects of the CVD process. Therefore, we developed a reduced gas-phase and surface chemistry for oxy-acetylene diamond CVD. The gas-phase combustion chemistry of oxy-acetylene flames was studied extensively, and a detailed reaction mechanism is available.[5] However, a generally accepted surface-reaction mechanism, based on elementary reactions, is still lacking.

Besides semiempirical diamond-growth models deduced for hot-filament conditions,[6,7] several authors have composed surface mechanisms for the growth on a diamond (100) surface.[8–10] Coltrin and Dandy[8] proposed a mechanism for growth on an unreconstructed dihydride diamond (100) surface. It is however, as the authors indicated, not an elementary mechanism that extends to a description of the detailed bond breaking and formation on a diamond (100) surface. Harris and Goodwin[9] and Ruf *et al.*[10] assume growth by the addition of gas-phase species to a (100)-(2×1) dimer carbon site. They assume that half the growth is accounted for by insertion of CH_3 into dimer bonds, while the other half is accounted for by the addition across a void between dimer bonds. Although the first assumption is supported by quantum-mechanical calculations by Skokov *et al.*,[11] the latter is not. Rather, Skokov *et al.*[11] found that migration of

[a)]Electronic mail: M.H.J.M.de.Croon@tue.nl

chemisorbed CH_2 groups on the diamond surface is the most likely route to fill voids between dimers.

Here we report the development of a detailed kinetic model for diamond growth on a (100) surface in an oxy-acetylene diamond CVD reactor, and the reduction of a detailed combustion mechanism. The surface mechanism includes both methyl radicals and acetylene as growth precursors. The surface processes are described in terms of elementary steps for which the kinetic data are based on quantum-mechanical calculations by Skokov *et al.*[11–13] No parameters were adjusted to describe experimental data.

II. GAS-PHASE MECHANISM

A. Reduction method

Wolden *et al.*[14] performed a reduction of the gas-phase chemistry in diamond growth methods from hydrocarbon–hydrogen mixtures. The resulting mechanism cannot be used when studying the present combustion based process. In combustion, the reduction of the mechanism for methane combustion, in particular, has been studied extensively.[15] A concise mechanism for acetylene-air flames has been proposed by Peters *et al.*[15] For the studied conditions it predicts that significant fractions of the combustion products consist of CO_2, while this is not predicted by more extensive mechanisms. Furthermore, Matsui *et al.*[16] present a mechanism for acetylene combustion which, however, does not include molecular oxygen. This is a key species for the combustion of acetylene.

Therefore we started the compilation of a gas-phase mechanism from the 48 species, 219 reactions combustion mechanism published by Miller and Melius[5] and applied for an oxy-acetylene flame by Meeks *et al.*[17] To maintain sufficient accuracy in the model calculations and simultaneously keep the computation time at a reasonable level, a reduction of the gas-phase mechanism was carried out under the conditions encountered in an oxy-acetylene flame.

The assumed reactor model for the reduction of the number of species in the gas-phase mechanism is a steady-state, one-dimensional (1D), laminar flame model simulated with the aid of the premixed flame code developed by Kee *et al.*[18] The free burning flame option was used, which means that the flow rate was adjusted until the position of the flame was fixed at a specified point. The determined inlet gas velocity is equal to the flame speed, defined as the speed at which a flame propagates through an open-ended horizontal tube. The model includes equations of conservation of mass and energy, and a balance equation for each species. It accounts for chemical reactions, species diffusion, and gas convection.

The operating conditions are derived from the conditions reported by Klein-Douwel *et al.*,[19] i.e., atmospheric pressure, an inflow temperature of 300 K and an acetylene excess S_{ac}, defined as the percentage of extra acetylene flow compared to the acetylene flow of a neutral flame,[19,20] of 5%. Here, as is found in practice,[19] a neutral flame is defined as a flame in which C_2H_2 and O_2 are fed in a 47.5:52.5 ratio.

A sensitivity analysis can be carried out by determining the normalized partial derivative for variable x_k, as a function of each reaction rate parameter, i.e., the pre-exponential factor of the Arrhenius temperature dependence A_i. The sensitivity coefficient $S_{k,i}$ of variable k for reaction i is defined as

$$S_{k,i}=\frac{A_i}{x_k}\frac{\partial x_k}{\partial A_i}. \tag{1}$$

It was evaluated for the temperature, the flame speed and the concentrations of H and CH_3. These particular species were chosen because they appear to play an important role on the diamond surface.[6] The temperature rises from 300 to 3500 K roughly between $x=2$ and $x=2.15$ mm from the burner exit. The sensitivity analysis was therefore carried out at $x=2.08$, 2.12 and 3.9 mm, i.e., at two points in the region of the steep temperature rise and one in the hot combusted gas zone. All the reactions for which one of the above mentioned variables had a high sensitivity coefficient were listed. From this list the set of important gas-phase species in an oxy-acetylene combustion torch reactor was obtained. For the subsequent testing of the reduced mechanism, all reactions containing species not included in this set were removed from the full mechanism.

TABLE I. Summary of the species contained in each mechanism. A cross indicates that the mechanism contains the named species.

Mechanism number:	I	II	III	IV
H, O, H_2, O_2, OH, CO, CO_2, HCO, HCCO, CH_2(s), CH_3, C_2H_2, C_2H_3	X	X	X	X
CH_2, C_3H_2, H_2CCCH, CH_4, C_2H, H_2O, C_2 H_2CCCCH, C_4H_2, CH	X	X	X	
CH_2O, C_2H_4, C_2H_5, CH_2CHCCH	X	X		
HO_2, H_2O_2, CH_2OH, CH_3O, HCCOH, CH_2CO, C, C_5H_2, C_6H_2 HCCHCCH, C_6H_5, C_6H_6, C_3H_4 C_3H_4P, C_6H_5O, $CH_2CHCHCH$, CH_2CHCCH_2, C_2O, H_2C_4O, $CH_2CHCHCH_2$, C_2H_6	X			
Number of species	48	27	23	13
Number of reactions	219	119	92	28
Flame speed (m/s)	6.4	6.2	6.3	4.2

B. Results

The full 48 species mechanism was reduced in three steps to a 13 species mechanism. The retained species in each of these reduction steps are listed in Table I. In Fig. 1 the CH_3 and H concentration profiles calculated with three reduced mechanisms are compared to those calculated with the full mechanism.

Of all species, the CH_3 concentration was found to be one of the species most sensitive to model reduction. In the 27 species mechanism, it deviates less than 10% from the full mechanism. Because CH_3 is an important species for diamond growth, this mechanism is used in the reactor simulations. By reducing to 23 species, the deviation of the CH_3

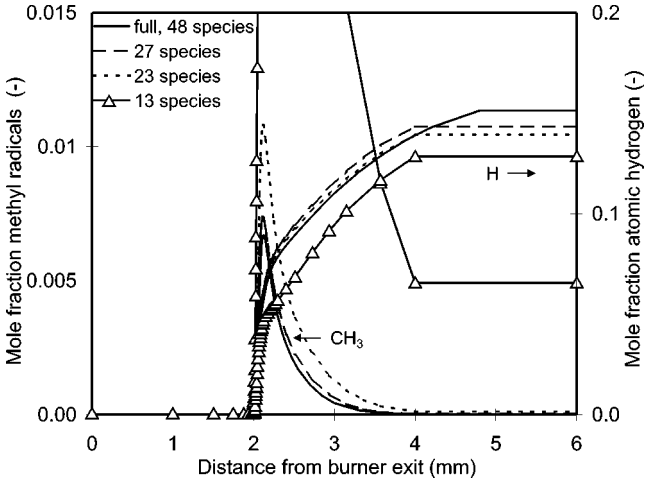

FIG. 1. Concentration profiles of the reduced mechanisms computed with the free-standing premixed flame model, compared to those of the full mechanism.

profile increases to a maximum of 50%, but the deviation in H and other main species profiles is still less than 10%. Finally, the 13 species mechanism, which only contains the reactants, products and the most important intermediates, still predicts the right trends but can be an order of magnitude off in the values predicted for the concentrations.

To test whether the 27 species mechanism can be applied under a broader range of conditions than those for which it has been reduced, it was compared to the full mechanism with the acetylene excess ranging from -10% to 20%. For lean flames with an acetyelene excess of -10% there is hardly any difference between the concentration profiles calculated with the full and with the reduced mechanism. For species present in significant concentrations (higher than 1 ppm) the profiles deviate a few percent at most. Deviations become larger when the flame becomes richer; species with a high carbon content, like C_2 and CH show large deviations. At an acetylene excess of 20%, the reduced mechanism overestimates the concentration of these species by a factor of 2. This can be explained from the reaction of these species to larger molecules in the full mechanism. At this acetylene excess the error the reduced mechanism causes is typically 30% for all other species.

Although there is a large influence of pressure on the concentration profiles, the error resulting from reducing the mechanism is not greatly affected by the pressure. Varying the pressure between 1 kPa and 1 MPa resulted in a combustion zone ranging from 10 mm at the lowest pressure to 20 μm for the highest. However, the difference between the concentration profiles predicted with the full mechanism and the reduced mechanism remained below 10% for the species that play an important role on the diamond surface.

C. Stagnation flow reactor model

The oxy-acetylene torch reactor was simulated with a one-dimensional stagnation flow CVD reactor model by Coltrin *et al.*[21] This model considers a solid surface of infinite extent separated from a parallel burner outlet by distance d, or in practice a surface of finite radius R and $r/R \ll 1$. A forced flow emerges from the outlet and is directed toward the solid surface. The axial velocity u, the radial velocity divided by the radial distance v/r, the gas-phase species mole fractions x_k, the species site fractions and the temperature T are all a function of the axial distance only.

TABLE II. Input data for the stagnation-flow reactor model.

		Standard settings	Range of variation
S_{ac}	(–)	5%	1%–10%
$T_{x=d}$	(K)	300	···
P	(Pa)	1×10^5	···
$u_{x=d}$	(m/s)	6	···
d	(mm)	1.2	0.9–2.0
T_{surf}	(K)	1400	1100–1500
Γ	(mol/m^2)	5.27×10^{-5}	···

To evaluate the effect of surface reactions on the gas-phase profiles, simulations were carried out with the addition of the surface mechanism as described in Sec. III. The input parameters are given in Table II. The length d is approximately equal to the flame tip-to-substrate distance because the flame is located directly behind the burner outlet.

Figure 2 shows that the addition of the surface mechanism has a large influence on the atomic hydrogen concentration profile in particular. This is caused by the high diffusivity of H. The effect of surface reactions on concentration profiles of larger molecules like CH_3 is less pronounced.

The effects of various reactor settings on the gas-phase and surface composition are studied in more detail in Sec. IV.

III. SURFACE REACTION MECHANISM

A. Construction

A surface reaction mechanism that predicts the growth rate of the diamond film was composed. It is based on the assumption that the rate limiting step is not the nucleation step for the growth of a new layer. This assumption is acceptable, because in practice the natural diamond that is used

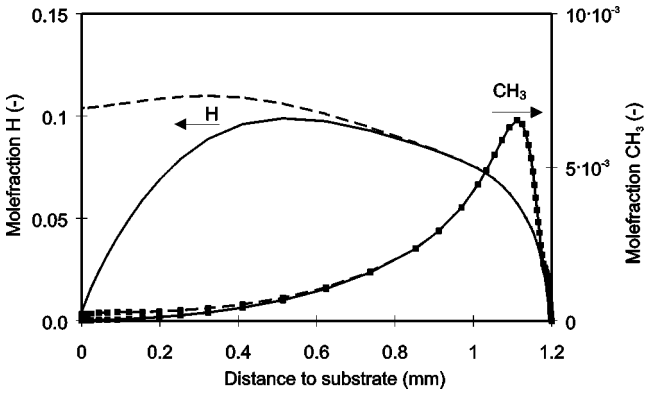

FIG. 2. Influence of the addition of a surface mechanism on concentration profiles computed with a stagnation flow reactor model. The dotted lines are calculated without addition of the surface mechanism, the solid lines with the surface mechanism. The input parameters are given in Table II.

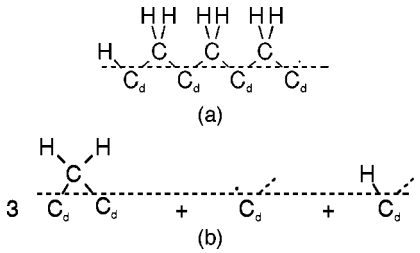

FIG. 3. Example of a component of the surface (a) and its subdivision into species (b). C_d denotes a carbon atom in the diamond lattice. The dotted line is the division between the diamond bulk and the surface.

as a substrate contains some defects. As a result, there are always enough steps on the surface to stop nucleation from being rate limiting.

The surface processes are modeled in terms of elementary chemical reactions. The reaction mechanism is based on the results of quantum-mechanical calculations by Skokov *et al.*,[11–13] who explored possible reaction steps responsible for diamond growth but did not present a complete reaction mechanism ready to be used in simulations.

Because our ultimate goal is to combine the surface mechanism with a multidimensional reactor model, the computation time required by the surface mechanism has to be limited. Therefore, we chose a surface mechanism that has the same structure as the gas-phase mechanism. This means that the mechanism consists of randomly distributed surface species that react with a rate proportional to the reactant concentrations. This corresponds to the so-called mean field approximation. It implies that the presence of a particular species on a site does not influence the distribution of the species on neighboring sites. For example, the component of the surface indicated in Fig. 3(a) is subdivided into the species indicated in Fig. 3(b).

The surface is subdivided into the species listed in Appendix A. The balances for the surface species are made on the basis of the total number of sites. Two bonds of each carbon atom on the (100) surface are attached to the diamond lattice. The other two bonds protrude in the direction of the gas phase. Since the total number of carbon atoms in the diamond lattice on the (100) surface is constant during growth, the number of bonds in the direction of the gas phase is too. One such bond will be called a site. The site density is the constant Γ.

A name has been assigned to each species on the surface. A species on which gas-phase species can absorb, defined as a site in Langmuir kinetics, is also considered a species and ''occupies'' a number of sites. For example, the dimer S2 to which 1 hydrogen atom is attached occupies four sites and consists of 1 hydrogen atom and 0 carbon atoms.

The mathematical formulation for the rate of reaction of gas-phase species with the surface and surface species is the same as that used in the Chemkin codes.[22] The rate constants are assumed to have an Arrhenius temperature dependence.

The complete surface reaction mechanism is presented in Appendix B. The gas-phase precursors of diamond are methyl radicals and acetylene molecules, which are regarded as the most important precursors.[1] They adsorb on dimer sites. The different configurations of a molecule consisting of 1 or 2 carbon atoms, and a varying number of hydrogen atoms, adsorbed on one or both diamond dimer carbon atoms, lead to a large number of surface species as presented in Appendix A.

Because growth occurs via adsorption to dimer sites, at least two different steps have to be distinguished: one for the insertion of a carbon atom into a dimer bond, and one for the closure of the void between two dimer bonds with a carbon atom. There are two different views concerning the latter step. Harris and Goodwin[9] and Ruf *et al.*[10] assume that first carbon atoms insert into the dimers, and then the void side is closed by adsorption of a CH_3 molecule to one of the two neighboring diamond carbon atoms. Skokov *et al.*,[11] however, calculated that this route is unfavorable due to large steric repulsions. They found that instead migration of a CH_2 group over the surface to close a void is feasible on kinetic and thermodynamic grounds. Therefore, we adopted this latter route in the present mechanism.

Methyl radicals adsorb on dimers as indicated in Fig. 4(a). Reactions (11)–(16) represent the adsorption of a methyl radical, its subsequent migration over the surface, and closure of a void. Reactions (17)–(21) correspond to the insertion of CH_3 into a dimer bond. A carbon is considered to be part of the diamond lattice when it has formed a dimer with another carbon atom, according to reaction (67). When the reactions in each part of the path are added, the conversion of CH_3 into diamond can be represented by three overall reactions: closure of a void

$$S2+S6+CH_3+2H \rightleftharpoons S4+S12+2H_2, \tag{2}$$

insertion into a dimer

$$S12+CH_3+2H \rightleftharpoons S4+S6+2H_2, \tag{3}$$

and closure of the dimer bond

$$2S4+3H \rightleftharpoons S2+2\text{diamond}+3H_2, \tag{4}$$

where S2 and S12 are the free sites in this mechanism.

Four of the kinetically most favorable routes[12] for diamond growth from acetylene are discussed in more detail here. Figure 4(b) depicts three of them: reactions (28)–(32), reactions (33)–(37) plus (31)–(32), and reaction (43)–(55). Via reactions (56)–(60), the top carbon atom is etched from an adsorbed acetylene molecule, after which the bottom carbon can be etched off as well or can be included in the diamond lattice in the same way as the methyl radical.

Apart from etching via the reverse of the growth route, carbon atoms can be etched with atomic hydrogen as illustrated in Fig. 4(c) or with oxygen as in Fig. 4(d).

Based mainly on the forward reaction rate constants and equilibrium constants presented by Skokov *et al.*,[11,12] a set of thermodynamic data was constructed. For the etching of carbon from the surface with oxygen, data from similar gas-phase reactions were obtained from the NIST library.[23]

Skokov *et al.*[11,12] do not supply enough reaction rate data for hydrogen abstraction and addition reactions to determine the entropy and enthalpy of the reaction. They state that hydrogen abstraction and addition reactions via

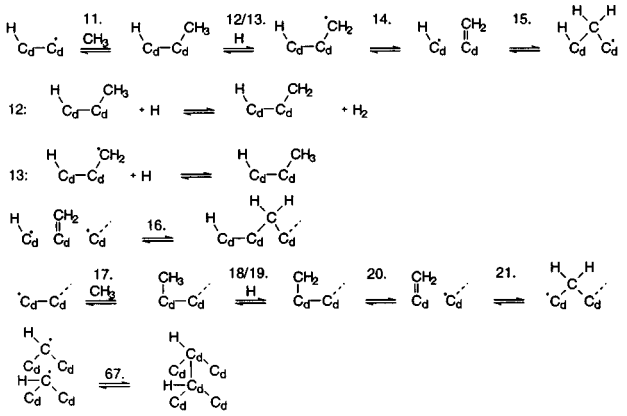

(a)

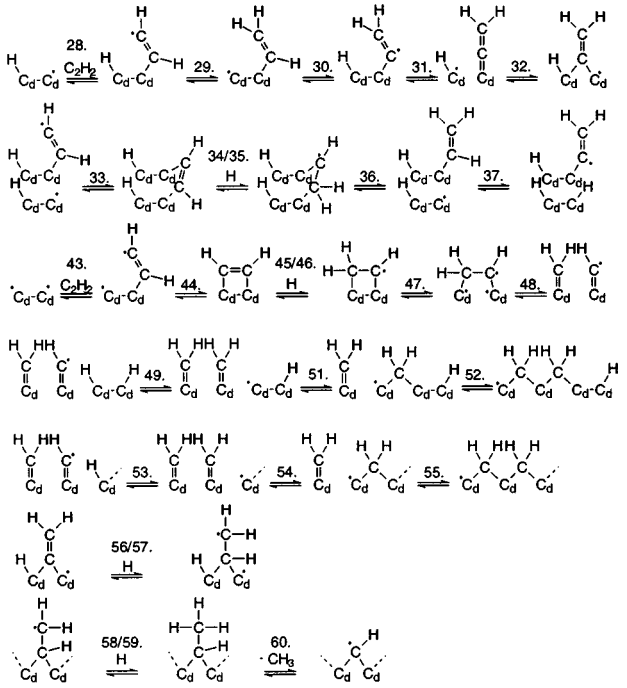

(b)

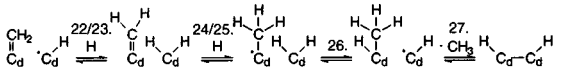

(c)

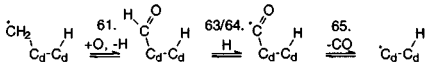

(d)

FIG. 4. Reaction routes for methyl radical adsorption(a) acetylene adsorption(b), etching of carbon with atomic hydrogen(c), or oxygen(d). The numbers correspond to the reaction numbers in Appendix B.

TABLE III. Enthalpy of reaction of various hydrogen abstraction reactions.

Abstraction of hydrogen from	$\Delta H/R$ (K)	Reaction no.	Ref.
C_2H_6	-3.0×10^3	12, 18, 59	32
S2	-7.8×10^3	2, 4, 9	24
S7	-15.2×10^3	6, 23	···
S4	-20.3×10^3	8	···
C_2H_5	-34.3×10^3	25, 35, 40, 46, 57	32
CH_3HCO	-9.2×10^3	63	32

$$C_dH+H\cdot\rightarrow C_d\cdot+H_2 \tag{5}$$

and

$$C_d\cdot+H\cdot\rightarrow C_dH \tag{6}$$

have rate constants of 10^6 $m^3\times mol^{-1}\times s^{-1}$and 10^7 $m^3\times mol^{-1}\times s^{-1}$, respectively, where C_d represents a carbon atom on or in the diamond lattice. In the literature the abstraction of hydrogen from a dimer was the only hydrogen abstraction reaction for which the reaction enthalpy ΔH can be found (see, e.g., Ref. 24). Thus enthalpies of hydrogen abstraction reactions have to be estimated with similar gas-phase reactions as a guideline. Table III lists the enthalpy of reaction for different hydrogen abstraction reactions as estimated in this study.

A complete, consistent set of thermodynamic data is now obtained by setting the enthalpy of formation H_i^0 of the dimer with 2 adsorbed hydrogen atoms to 0.785 kJ/mol[25] and the entropy of formation of the dimer without adsorbed hydrogen to zero. The enthalpy and entropy of the gas-phase species were calculated at 1400 K, the typical temperature at which diamond is deposited in combustion-flame diamond CVD.[19] The entropy and enthalpy of formation of the remaining surface species were then calculated with the aid of the heat of reaction data as described above. Because no temperature dependence of the enthalpy and entropy of reaction is known, the enthalpy and entropy of the surface species were assumed to be constant. The resulting set of thermodynamic data can be found in Appendix A.

B. Test of the surface mechanism

The surface chemistry was studied separately from the gas-phase chemistry, using a perfectly stirred reactor model with surface reactions.[22] The residence time τ was selected to be small enough to ensure that the composition of the gas in the reactor was nearly the same as the composition of the inlet gas. The latter was estimated with the aid of the calculations in the stagnation point flow model (Sec. II C). The input parameters for the perfectly stirred reactor model are listed in Table IV.

Verification of the surface chemistry mechanism, separate from the gas-phase mechanism, is hampered by a lack of experimental data on the growth rates on a (100) surface as a function of the temperature and the gas-phase composition directly above the surface. In practice, the growth rates are measured on mixed (111) and (100) oriented surfaces, as a function of the surface temperature and the inlet composition.[20] Nevertheless certain trends are visible.

TABLE IV. Input data for the perfectly stirred tank reactor model including surface reactions. Concentrations are estimated with the aid of the stagnation flow model.

		Standard settings	Range of variation
τ	(s)	1×10^{-8}	⋯
P	(Pa)	1×10^{5}	⋯
x_{CH_3}	(mole frac.)	3×10^{-4}	3×10^{-5}–3×10^{-4}
$x_{C_2H_2}$	(mole frac.)	4.4×10^{-4}	3×10^{-5}–1×10^{-3}
x_H	(mole frac.)	4.5×10^{-3}	3×10^{-4}–1×10^{-2}
x_O	(mole frac.)	2.8×10^{-6}	⋯
x_{H_2}	(mole frac.)	0.276	⋯
x_{CO}	(mole frac.)	remainder	⋯
T	(K)	1400	1100–1500
a_{surf}	(m^2_{surf}/m^3_{reac})	1.5	⋯
Γ	(mol/m^2)	5.27×10^{-5}	⋯

Schermer *et al.*[20] have measured the growth rate in an oxy-acetylene combustion torch reactor on the order of 100 μm/h or 30 nm/s, increasing as a function of the temperature up to approximately 1400 K, above which it becomes constant.

The growth rate as a function of temperature and atomic hydrogen concentration, predicted by the proposed mechanism, is plotted in Fig. 5. The growth rate increases with temperature until approximately 1300 K, after which it becomes close to constant, similar to the temperature dependence found by Schermer *et al.*

To capture the dependence of the growth rate on the concentrations of H, CH_3 and C_2H_2, each concentration was varied as indicated in Table IV, while the other variables were kept at their standard value. The resulting growth rates are presented in Fig. 6. The model predicts that the growth rate is between the zeroth and first order in the H concentration, and decreases in order as the H concentration increases. Furthermore, an almost linear increase of the growth rate with the CH_3 concentration is predicted. This corresponds well with the model of Goodwin,[6] who deduced the following proportionality from a simplified model of the gas-surface chemistry for the growth rate:

$$\frac{[CH_3]\times[H]}{(\text{constant}+[H])}. \tag{7}$$

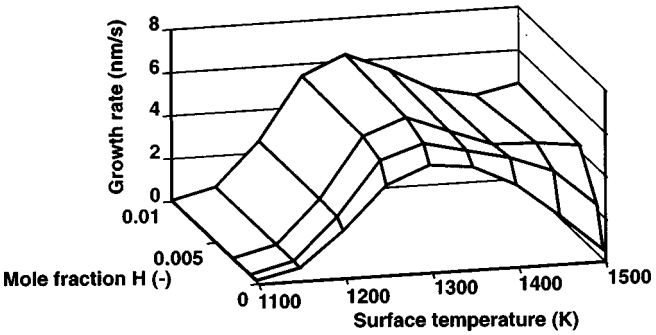

FIG. 5. Dependence of the diamond growth rate on the atomic hydrogen concentration and surface temperature. The applied conditions are listed in Table IV.

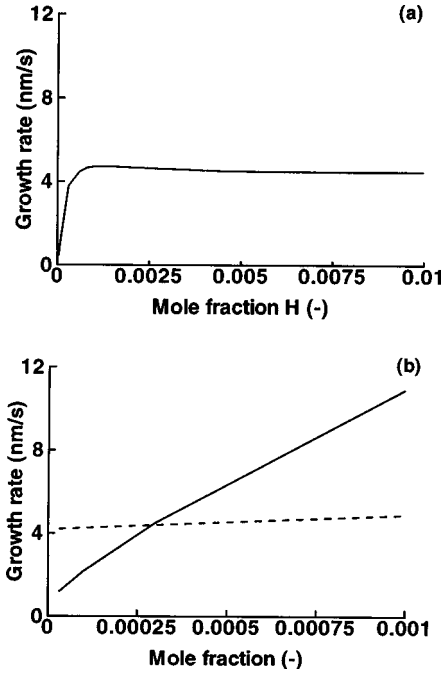

FIG. 6. Dependence of the diamond growth rate on (a) H and (b) CH_3 (solid line) and C_2H_2 (dashed line) concentrations. All variables except the varied concentrations were kept at their standard value (Table IV).

A weak positive dependence of the growth rate on the C_2H_2 concentration is found.

The reliability of the surface mechanism is partly dependent on the reliability of the predicted surface composition. In Table V the predicted composition of the surface is given and in Fig. 7 this composition is used to compile an image of the surface under oxy-acetylene torch conditions. It shows that the surface is hardly recombined and that there are on average about 1.75 hydrogen atoms per carbon atom. The reason for this is that the concentration of CH_3 and the adsorption enthalpy of CH_3 on a dimer have such high values, that the equilibrium is strongly in the direction of the adsorbed species ($K=S8/(CH_3\times\ S2)=2\times10^7\ mol^{-1}\times m^3$). This leads to a low dimer concentration. Because no *in situ* measurements are available, this surface composition cannot be verified. However, Winn *et al.*[26] predicted that at lower

TABLE V. Sensitivity of the growth rate (G) to the heat of formation of species i (H_i^0) of the species with an absolute sensitivity coefficient higher than one. The gas phase composition was the standard gas-phase composition (Table IV). Also shown is the surface coverage under the same conditions.

Species	$(H_i^0/G)(\partial G/\partial H_i^0)$	Coverage
S4	116	69%
S8	51	0.01%
S1	−19.7	2%
S2	6.7	0.3%
S13	−4.5	0.01%
S5	−4.3	21%
S35	−3.65	<0.01%
S36	−3.17	<0.01%
S19	−1.8	<0.01%
S11	−1.8	2%

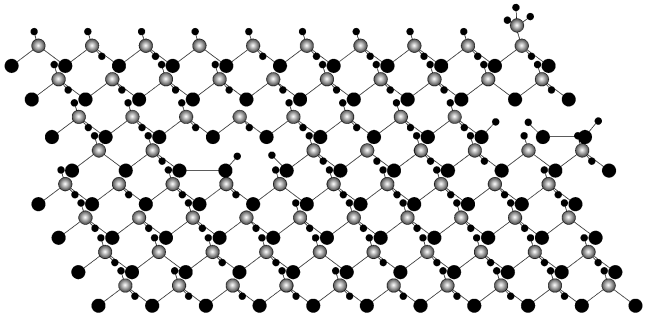

FIG. 7. Compilation of the surface based on the composition predicted by the mechanism under oxy-acetylene CVD conditions. The large spheres indicate carbon atoms (black: lower layer, gray: upper layer), the small spheres indicate hydrogen atoms. The bond lengths and angles do not necessarily correspond to reality.

temperatures a surface coverage of 1.5–2 hydrogen atoms per carbon atom is energetically most favorable if the surface is in contact with a gas consisting of atomic and molecular hydrogen. When the acetylene concentration is set to zero and the CH_3 and H concentrations are reduced to a mole fraction of 1×10^{-6}, the number of hydrogen atoms per carbon atom decreases to 1. This is in agreement with the literature.[26] Thus, the surface structure predicted with the developed mechanism appears to be a physically realistic structure.

C. Sensitivity analysis heat of formation

As stated, no heat of reaction is given in the literature for most hydrogen abstraction reactions. Moreover, these heats of reaction are probably not constant but dependent on surface coverage. Therefore, a sensitivity analysis was carried out. Table V lists the species for which a change of 5% in their heat of formation caused the growth rate to change more than 5%. The heat of formation of the same species had a large effect on the surface composition.

Of the first three species in Table V, the enthalpy of formation of S8 and S1 are relatively reliable. As explained earlier, the heat of formation of S1 formed the basis for the calculation of all other heats of formation. Increasing its value would lead to an increase with the same amount of all other heats of formation, and thus there would be no net effect on the growth rate. The heat of formation of S8 is linked via two well-studied reactions to S1. This is not the case for the species S4. The value of its heat of formation is probably dependent on the surface coverage with S4. Therefore, for an improvement of the surface mechanism it would be rewarding to study the heat of formation of species S4 and its dependence on the surface coverage.

D. Comparison of the reaction routes

Figure 8 shows the routes through which the diamond layer grows according to the surface mechanism. The left part of the scheme, which accounts for the adsorption of CH_3, is presented in more detail in Fig. 9. The left part of Fig. 9 corresponds to Eq. (3), the middle part to Eq. (2), and

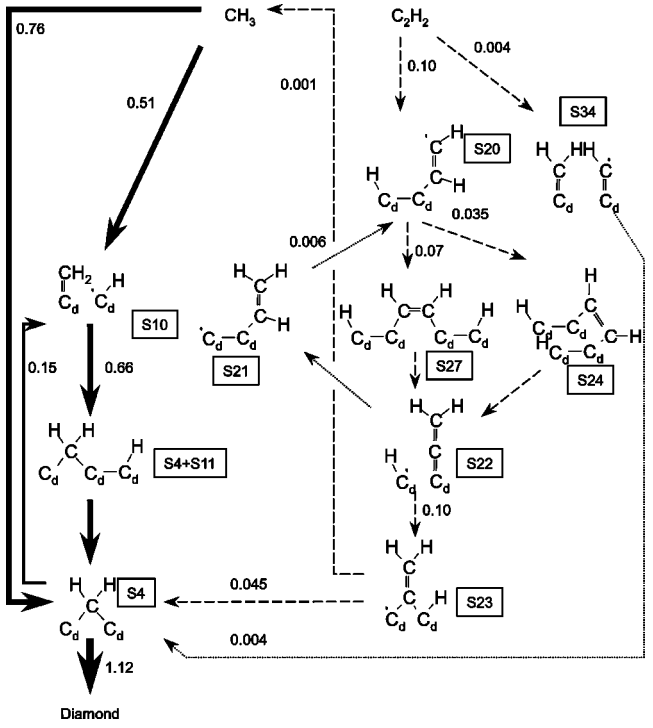

FIG. 8. Comparison of the reaction routes on the surface that lead to growth. The reaction rates are in mmol carbon on the surface per square meter per second. Values are calculated under the standard growth conditions (Table IV).

the bottom right part to Eq. (4). Discrepancies in the species balances in this figure can be ascribed to disregarding the C_2H_2 adsorption routes.

Figure 9 shows that the migration reactions (15) and (16) are nearly at equilibrium. This accounts for the monocrystalline growth of diamond. A sensitivity analysis was carried out at the standard settings as indicated in Table IV. It appeared that the growth rate is especially sensitive to the preexponential factor of the adsorption of CH_3 [reaction (11) and (17)] and the intermediate hydrogen abstraction reaction

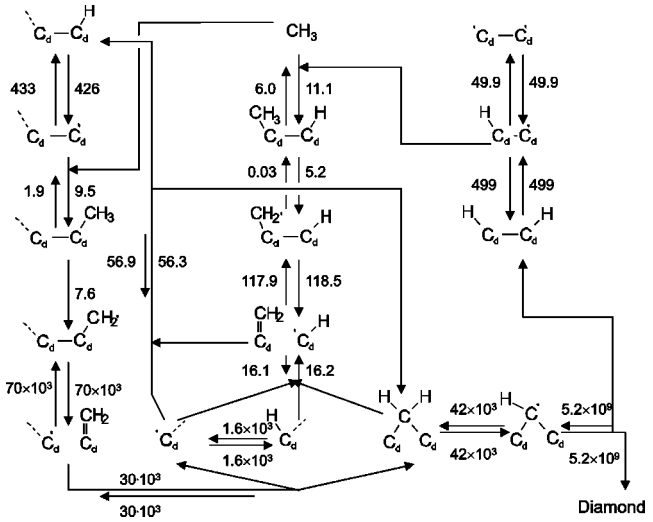

FIG. 9. Detailed view of the part of the reaction mechanism that accounts for the growth via CH_3. Reaction rates are in mmol/m^2/s.

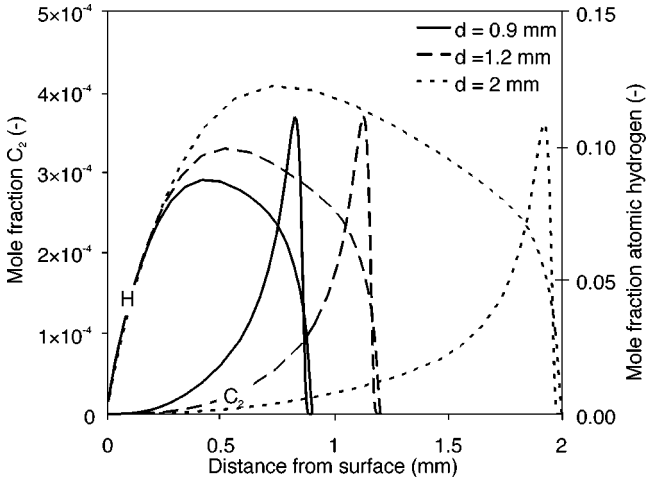

FIG. 10. Effect of the increase of the flame tip-to-substrate distance on the C_2 and H concentration profiles under the conditions as in Table II.

[reaction (12)]. Figure 9 shows that these are the steps for which the net forward reaction rate is largest in comparison with the total forward rate. Furthermore, the growth rate is sensitive to the intermediate surface reaction [reaction (51)] and the acetylene adsorption step [reaction (28)]. The listed steps account for the positive order in the methyl radical, atomic hydrogen and acetylene concentrations. At higher acetylene super saturations the sensitivity for reaction (28) increases. The reason for this is that the contribution of acetylene to the growth rate increases. At decreasing molecular hydrogen concentrations the sensitivity coefficient for hydrogen abstraction reactions increases.

To answer the question of which of the two species—CH_3 or C_2H_2—is the most important precursor to diamond, the net adsorption of CH_3 has been compared to that of C_2H_2. It appears that, although the mole fraction of C_2H_2 in the gas phase directly above the surface is a factor of two higher than the mole fraction of CH_3, the methyl radical accounts for 95% of the growth at an acetylene super saturation of 5%. This means that under flame conditions CH_3 is approximately 40 times more reactive than C_2H_2. Experimentally it was found, that for different kinds of reactors CH_3 is 10–100 times more reactive than C_2H_2.[27–29]

Although quantum-mechanical calculations of adsorption were only carried out for the species C_2H_2 and CH_3, they are not the only species that could be growth precursors. The minimum mole fraction of a species necessary to account for growth rates on the order of 30 nm/s is 10^{-6}, assuming a sticking coefficient of one. From the species with two or less carbon atoms CH_4, CH_3, C_2H_2, CO_2, CO and C_2H_3 meet this condition. C_2 for example, for which a correlation has been found with the growth rate,[19] has a concentration that is too low for it to be able to significantly contribute to diamond growth. From the species that meet the concentration condition, CO_2, CO and CH_4 are too stable to be a growth precursor, which leaves C_2H_2, CH_3 and C_2H_3. The concentration of C_2H_3 is two orders lower than the CH_3 concentration, while there is no reason to expect that its reactivity is two orders greater.

Addition of oxygen to a diamond CVD reactor generally leads to a decrease of the growth rate and an increase of the diamond quality.[30] This could be caused by either an interaction of molecular or atomic oxygen with the diamond surface, or by a change in gas-phase composition. To test the first hypothesis, the influence of the etching of carbon by O and O_2 via reactions (61)–(66) (Appendix B) has been compared to other etching routes.

The mole fractions of O and O_2 are on the order of 10^{-6}, which is high enough for them to play a significant role. If the etching via different routes is compared, O and O_2 etch only a fraction of 10^{-4} and 10^{-8}, respectively, of the total amount of carbon that is etched from the surface. However, most CH_3 desorbs from the surface through reaction (60). This is the desorption of the top carbon atom from an acetylene molecule for which no analogous route with atomic oxygen is provided. If this etching step is not taken into account, atomic oxygen is slightly more effective—relative to its concentration—than atomic hydrogen in etching carbon from the surface. This is caused by the higher desorption enthalpy of CH_3 compared to CO. However, because of its low concentration, atomic oxygen does not contribute significantly to carbon etching.

The number of species in the surface mechanism can be reduced by comparing the various reaction paths. The routes that least contribute to growth can be identified from Figure 8. Growth from acetylene via species S21 and S34 does not appear to be significant. At higher acetylene super saturations, acetylene contributes via species S24 and S27 up to 25% to the growth at a super saturation of 10%. These routes can therefore not be neglected. Etching via S28 only constitutes 2.5% of the total etching and is negligible, like etching with atomic and molecular oxygen. The same conclusions can be drawn from the sensitivity analysis. Thus reactions (22)–(27), (30)–(31), (43)–(48) and (61)–(66) and the corresponding species can be removed from the mechanism without large deviations in the results.

IV. COMBINATION OF THE GAS-PHASE AND SURFACE REACTION MECHANISM

The gas-phase and the surface mechanism are combined with transport equations to yield a one-dimensional reactor

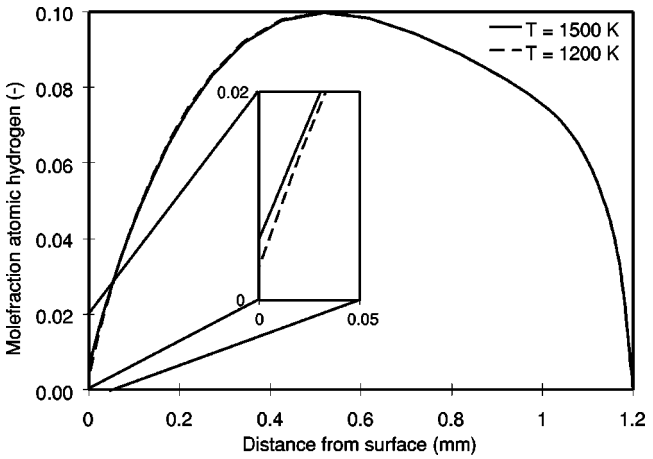

FIG. 11. Atomic hydrogen profiles calculated with the stagnation flow reactor model at two different surface temperatures.

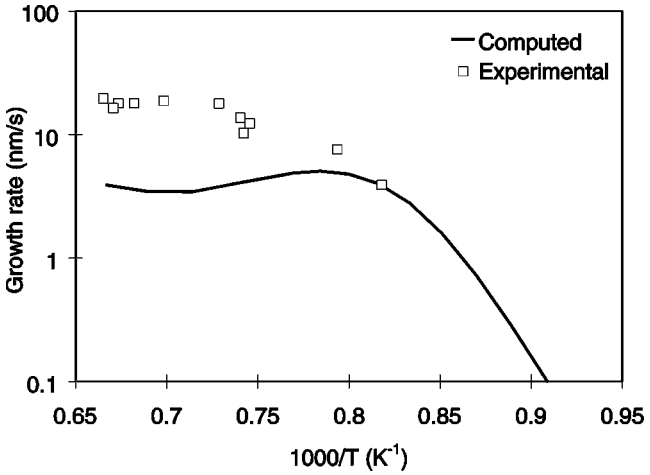

FIG. 12. Comparison of the predicted temperature dependence of the growth rate to the measured dependence (Ref. 20). The growth rates were measured on a combined (100)-(111) oriented polycrystalline surface.

model. Thus the influence of reactor settings can be studied and compared to experimental results. Here, the surface temperature, the acetylene–oxygen ratio, and the distance between the flame front and the surface are varied. The input parameters are given in Table II.

In an earlier publication we have shown that the shapes of the concentration profiles predicted by this model at small flame tip-to-substrate distances (1 mm) correspond reasonably well to that of the measured profiles.[31] According to the present 1D simulations, the influence of the flame tip-to-surface distance on the concentration profiles is not very strong. The effect of an increase of the distance is that the profiles become somewhat elongated (see Fig. 10). In practice, however, the effect of increasing the flame tip-to-substrate distance is expected to be dominated by two-dimensional (2D) effects like in-diffusion of air and the conical shape of the flame, which is not included in the current simulations. A 2D model should give more reliable predictions for effects of variation of the reactor geometry.

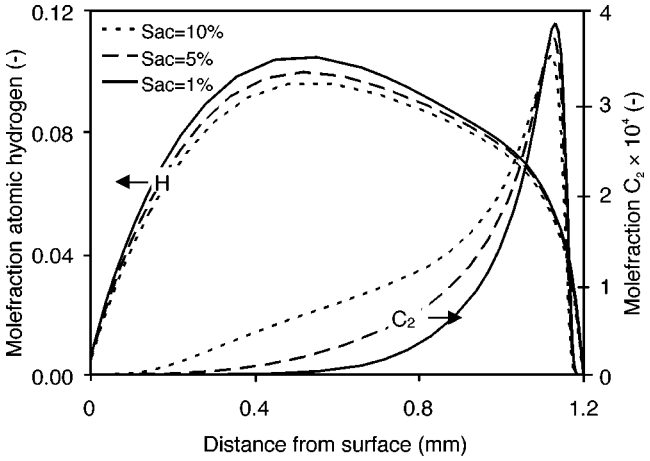

FIG. 13. Molecular hydrogen and C_2 profiles calculated with the stagnation flow reactor model with a varying acetylene excess in the feed.

TABLE VI. Influence of the acetylene excess on the composition near the surface.

Species	3%	5%	7%	10%
H_2	0.267	0.277	0.285	0.288
H	4.63×10^{-3}	4.47×10^{-3}	4.27×10^{-3}	4.15×10^{-3}
CH_3	5.72×10^{-5}	2.08×10^{-4}	3.84×10^{-4}	4.25×10^{-4}
C_2H_2	5.09×10^{-5}	4.46×10^{-4}	2.35×10^{-3}	7.11×10^{-3}

A. Influence of the surface temperature

The substrate temperature does not appear to have a large influence on the gas-phase composition. To illustrate this, the atomic hydrogen profile is plotted in Fig. 11 for substrate temperatures of 1200 and 1500 K. The profiles start to differ only very close to the surface. At the surface, the H concentration increases by a factor of 2 when the temperature is raised from 1200 to 1500 K.

Growth rates were compared to the experimentally measured values in Fig. 12. Considering that no parameters were adjusted to fit the data, the model predicts the growth rate fairly well. Both the experiments and the model show an initial increase with temperature and a constant growth rate at higher temperatures. The difference can possibly be ascribed: (i) to the fact that the surface mechanism, valid for a monocrystalline (100) oriented surface, was compared to growth data from a polycrystalline mixed (100) and (111) oriented surface, (ii) to uncertainties in the thermodynamic data set as described previously and (iii) to 2D effects that were not included in the model.

B. Influence of the acetylene–oxygen ratio

A change in the acetylene–oxygen ratio does lead to a significant change in the gas-phase concentration profiles (see Fig. 13). An increase of acetylene super saturation changes H and CH_3 concentrations, but the most important influence is on the acetylene concentration above the surface (see Table VI). The overall effect is an increase of the growth rate (Fig. 14) with an increasing acetylene super satu-

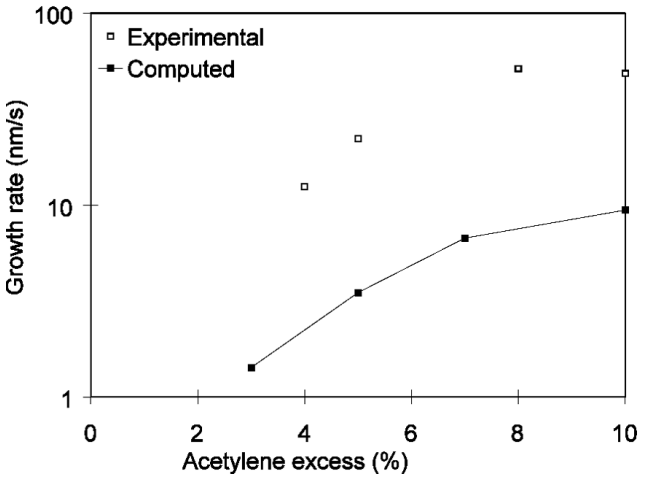

FIG. 14. Comparison of the predicted dependence of the growth rate on the acetylene excess and the measured dependence (Ref. 20). The growth rates were measured on a combined (100)-(111) oriented polycrystalline surface.

ration in the feed. Both the experimentally measured and the computed growth rates increase approximately linearly with the acetylene super saturation. In absolute values they differ by about a factor of 5.

V. CONCLUSIONS

A 48 species, 219 reaction gas-phase combustion mechanism was reduced to a 27 species, 119 reaction mechanism, resulting in concentration profiles that deviated under oxy-acetylene diamond CVD conditions by at most 10% from those obtained with the full mechanism. A detailed surface mechanism was compiled based on literature quantum-mechanical calculations. The surface reaction steps that did not contribute significantly to diamond growth were omitted from the mechanism. This resulted in a surface mechanism of 31 species and 45 reactions.

The combination of the surface and gas-phase chemistry mechanisms without any adjustments to kinetic parameters in a 1D stagnation model resulted in predictions that agree qualitatively well with measurements. The predicted growth rates are of the same order of magnitude as the measured growth rates, the predicted surface is physically realistic and experimentally observed trends in growth rate are reproduced.

Comparing growth via the methyl radical and via acetylene, it was found that the latter contributed to only about 5% of the growth, even though its concentration is an order of magnitude higher than the methyl radical concentration. Although atomic oxygen etches carbon from the surface more efficiently than atomic hydrogen, its low concentration makes it play a negligible role on the diamond surface in the oxy-acetylene combustion reactor.

The gas-phase and surface mechanism developed here are reliable and compact enough to be used in further 2D modeling to study the reactor geometry and the indiffusion of air into the flame.

APPENDIX A: LIST OF ALL SURFACE COMPONENTS AND THEIR THERMODYNAMIC PROPERTIES

H/R is the heat of formation under standard conditions divided by the universal gas constant (10^3 K). *S/R* is the entropy of formation divided by the universal gas constant (-).

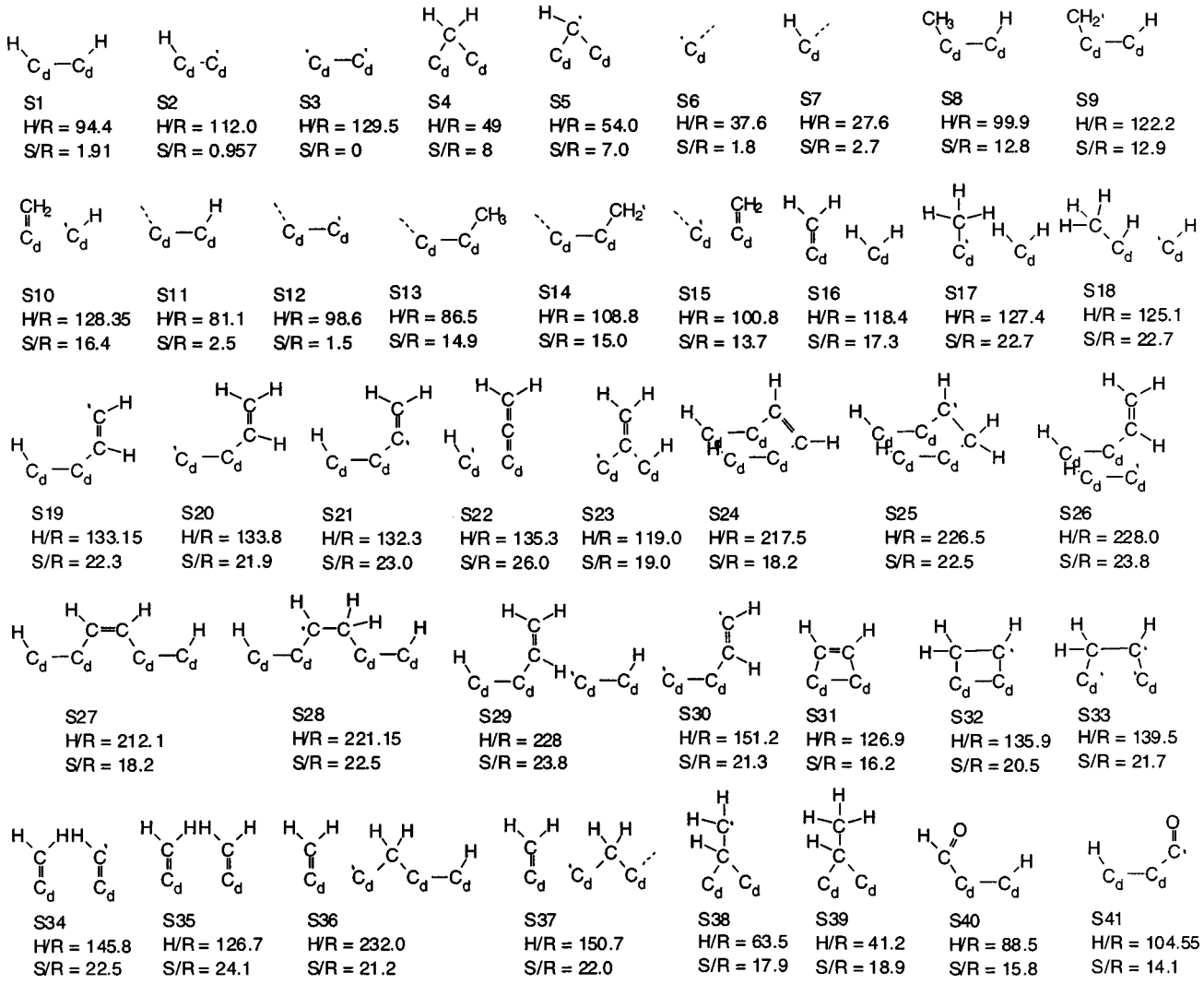

APPENDIX B: SURFACE REACTION MECHANISM FOR GROWTH ON (100)-ORIENTED DIAMOND

		A_i[a] (mol, m, s)	E_i (kJ/mol)
Hydrogen abstraction reactions			
(1)	S3+H⇌S2	6×10^{7}	0.0
(2)	S2+H⇌S3+H_2	3×10^{6}	0.0
(3)	S2+H⇌ S1	3×10^{7}	0.0
(4)	S1+H⇌S2+H_2	6×10^{6}	0.0
(5)	S6+H ⇌S7	3×10^{7}	0.0
(6)	S7+H⇌S6+H_2	3×10^{6}	0.0
(7)	S5+H⇌S4	3×10^{7}	0.0
(8)	S4+H⇌S5+H_2	6×10^{6}	0.0
(9)	S11+H⇌S12+H_2	3×10^{6}	0.0
(10)	S12+H⇌S11	3×10^{7}	0.0
Adsorption of a methylradical to S2			
(11)	S2+CH_3⇌S8	1.0×10^{7}	0.0
(12)	S8+H⇌S9+H_2	9×10^{6}	0.0
(13)	S9+H⇌S8	3×10^{7}	0.0
(14)	S9⇌S10	9.4×10^{12}	64.0
(15)	S10⇌S4+S7+S6	1.1×10^{12}	51.4
(16)	S6+S10⇌S4+S11	1.06×10^{18}	13.4
Adsorption of a methylradical to S12			
(17)	S12+CH_3⇌S13	1.0×10^{7}	0.0
(18)	S13+H⇌S14+H_2	9×10^{6}	0.0
(19)	S14+H⇌S13	3×10^{7}	0.0
(20)	S14⇌S15	9.4×10^{12}	0.0
(21)	S15⇌S4+S6	1.1×10^{12}	9.6
Etching of a methyl radical			
(22)	S10+H⇌S16	3×10^{7}	0.0
(23)	S16+H⇌S10+H_2	3×10^{6}	0.0
(24)	S16+H⇌S17	3×10^{7}	0.0
(25)	S17+H⇌S16+H_2	9×10^{6}	0.0
(26)	S17⇌S18	1.2×10^{12}	29.3
(27)	S28⇌S1+CH_3	3×10^{9}	30.1
Adsorption of acetylene to S2			
(28)	S2+C_2H_2⇌S19	7.9×10^{6}	35.1
(29)	S19⇌S20	2.45×10^{11}	85.3
(30)	S20⇌S21	1.3×10^{12}	139.6
(31)	S21⇌S22	25.4×10^{12}	36.8
(32)	S22⇌S23	7.97×10^{10}	31.4
Adsorption of acetylene to neighboring dimers			
(33)	S19+S2⇌S24	7.0×10^{15}	7.1
(34)	S24+H⇌S25	6×10^{7}	0.0
(35)	S25+H⇌S24+H_2	6×10^{6}	0.0
(36)	S25⇌S26	1×10^{7}	0.0
(37)	S26⇌S1+S21	1.3×10^{12}	84.9
(38)	S19+S2⇌S27	7.0×10^{15}	2.9
(39)	S27+H⇌S28	6×10^{7}	0.0
(40)	S28+H⇌S27+H_2	6×10^{6}	0.0
(41)	S28⇌S29	1×10^{7}	0.0
(42)	S29⇌S1+S21	1.3×10^{13}	84.9
Adsorption of both carbon atoms of acetylene to one dimer			
(43)	S3+C_2H_2⇌S30	7.8×10^{6}	28.8
(44)	S30⇌S31	4.17×10^{11}	9.6
(45)	S31+H⇌S32	6×10^{7}	0.0
(46)	S32+H⇌S31+H_2	6×10^{6}	0.0
(47)	S32⇌S33	38×10^{12}	48.9
(48)	S33⇌S34	40×10^{12}	118.7
(49)	S34+S2⇌S35+S3	3.93×10^{17}	117.5
(50)	S34+S1⇌S35+S2	3.93×10^{17}	117.5
(51)	S2+S35⇌S36	2.0×10^{16}	62.3
(52)	S36→S6+2S4+S11	1.1×10^{12}	13.4
(53)	S34+S7⇌S35+S6	1.14×10^{17}	97.0
(54)	S35+S6⇌S37	2.1×10^{16}	13.4
(55)	S37⇌S6+2S4	1.1×10^{12}	13.4
Etching of the top carbon atom from adsorbed acetylene			
(56)	S23+H⇌S38+S6+S7	3×10^{7}	0.0
(57)	S6+S7+S38+H⇌S23+H_2	1.08×10^{15}	0.0
(58)	S38+H⇌S39	3×10^{7}	0.0
(59)	S39+H⇌S38+H_2	9×10^{6}	0.0
(60)	S39⇌S5+CH_3	4.2×10^{15}	286.3
Etching with molecular and atomic oxygen			
(61)	S9+O⇌S40+H	8.0×10^{7}	0.0
(62)	S9+O_2⇌S40+OH	6.0×10^{3}	0.0
(63)	S40+H⇌S41+H_2	4.0×10^{7}	17.6
(64)	S41+H⇌S40	3×10^{6}	0.0
(65)	S41⇌CO+S2	1×10^{12}	52.7
(66)	S10+O⇌S1+HCO	1.2×10^{6}	37.6
Inclusion of surface carbon in the diamond lattice			
(67)	2 S5⇌2 Diamond+S1	1.69×10^{16}	0.0

[a]The unit of A_i depends on the order of the reaction. Concentrations of surface and gas phase species are in mol$\times$m^{-2} and mol$\times$m^{-3}, respectively. The reverse reaction rates can be calculated with the aid of thermochemistry.

[1] K. Spear and J. Dismukes, *Synthetic Diamond, Emerging CVD Science and Technology* (Wiley, New York, 1994).
[2] C. Johnston, Chimicaoggi **14**, 17 (1996).
[3] J. Schermer, W. v. Enckevort, and L. Giling, Diamond Relat. Mater. **3**, 408 (1994).
[4] T. Mountziaris, S. Kalyanasundaram, and N. Ingle, J. Cryst. Growth **131**, 283 (1993).
[5] J. Miller and C. Melius, Combust. Flame **91**, 21 (1992).
[6] D. Goodwin, J. Appl. Phys. **74**, 6888 (1993).
[7] D. Dandy and M. Coltrin, J. Mater. Res. **10**, 1993 (1996).
[8] M. Coltrin and D. Dandy, J. Appl. Phys. **74**, 5803 (1993).
[9] S. Harris and D. Goodwin, J. Phys. Chem. **97**, 23 (1993).
[10] B. Ruf, F. Behrendt, O. Deutschmann, and J. Warnatz, Surf. Sci. **352–354**, 602 (1996).
[11] S. Skokov, B. Weiner, and M. Frenklach, J. Phys. Chem. **98**, 7073 (1994).
[12] S. Skokov, B. Weiner, and M. Frenklach, J. Phys. Chem. **99**, 5616 (1995).
[13] S. Skokov B. Weiner, M. Frenklach, Th. Frauenheim, and M. Sternberg, Phys. Rev. B **52**, 5426 (1995).
[14] C. Wolden, K. Gleason, and J. Howard, Combust. Flame **96**, 75 (1994).
[15] N. Peters and B. Rogg, *Reduced Kinetic Mechanisms for Applications in Combustion Systems* (Springer, Berlin, Germany, 1993).
[16] Y. Matsui, H. Yabe, and Y. Hirose, Jpn. J. Appl. Phys., Part 1 **29**, 1552 (1990).
[17] E. Meeks, R. Kee, D. Dandy, and M. Coltrin, Combust. Flame **92**, 144 (1993).
[18] R. Kee, J. Grcar, M. Smooke, and J. Miller, A FORTRAN program for modeling steady laminar one-dimensional premixed flames, Sandia National Laboratories (1988).
[19] R. Klein-Douwel, J. Spaanjaars, and J. ter Meulen, J. Appl. Phys. **78**, 2086 (1995).

[20] J. Schermer, J. E. M. Hogenkamp, G. C. J. Otter, G. Janssen, W. J. P. van Enckevort, and L. J. Giling, Diamond Relat. Mater. **2**, 1149 (1993).
[21] M. Coltrin *et al.*, SPIN (version 3.83): A FORTRAN program for modelling one-dimensional rotating disk/stagnation-flow chemical vapour deposition reactors, Sandia National Laboratories (1993).
[22] H. Moffat *et al.*, Surface PSR: A fortran program for modelling well-stirred reactors with gas and surface reactions, Sandia National Laboratories (1991).
[23] W. Mallard, F. Westley, J. Herron, and R. Hampson, NIST chemical kinetics database, version 6.0, NIST standard reference data (Gaithersburg, MD, 1994).
[24] B. Weiner, S. Skokov, and M. Frenklach, J. Chem. Phys. **102**, 5486 (1995).
[25] D. Huang and M. Frenklach, J. Phys. Chem. **96**, 1868 (1992).
[26] M. Winn, M. Rassinger, and J. Hafner, Phys. Rev. B **55**, 5364 (1997).
[27] C. Johnson and A. Wayne, J. Electrochem. Soc. **141**, 2161 (1994),
[28] L. Martin, J. Mater. Sci. Lett. **12**, 246 (1993).
[29] J. S. Foord, K. P. Loh, N. K. Singh, R. B. Jackman, and G. J. Davies, J. Cryst. Growth **164**, 208 (1996).
[30] P. Bachmann, D. Leers, and H. Leers, Diamond Relat. Mater. **1**, 1 (1991).
[31] M. Okkerse *et al.*, in *Chemical Vapour Deposition*, Proceedings of the Fourteenth International Conference and EUROCVD-11, edited by M. Allendorf and C. Bernard (Electrochemical Society, Pennington, New Jersey, 1997), p. 163.
[32] R. Kee, F. Rupley, and J. Miller, The chemkin thermodynamic database, Sandia National Laboratories (1989).